TiO$_2$ NANOPARTICLES DECORATED FLOWER-LIKE MoS$_2$ NANOSPHERES WITH ENLARGED INTERLAYER SPACING OF (002) PLANE FOR ENHANCED TRIBOLOGICAL PROPERTIES

W. XU[a], Y. FU[b], W. YAN[b], Y. XU[b], M. XUE[a], J. XU[b*]

[a] *Changzhou Institute of Industry Technology, Changzhou, Jiangsu 213164, P.R. China*
[b] *School of physics and electrical engineering, Jiangsu University, Zhenjiang, Jiangsu province, 212013, P.R. China*

In this work, TiO$_2$@MoS$_2$ heterojunction of TiO$_2$ nanoparticles decorated MoS$_2$ nanospheres were successfully fabricated by one-step hydrothermal approach using TiO$_2$ as the precursor, and systematically investigated by various characterization methods (e.g. XRD, SEM, TEM and XPS analysis). Moreover, the tribological experiments of liquid paraffin contained TiO$_2$, MoS$_2$, and TiO$_2$@MoS$_2$ nano-additives were comparatively investigated by a ball-plate wear instrument, which tribological variables include applied load and rotational speed. TiO$_2$@MoS$_2$ as an additive in base oil exhibited superior antifriction and wear resistant among various nano-additives. At the optimal conditions, 5%-TiO$_2$@MoS$_2$-paraffin samples show the lower friction coefficient (~0.08) compared with pure paraffin, and paraffin contained TiO$_2$ and/or MoS$_2$. Additionally, the excellent anti-friction and wear-resistant of TiO$_2$@MoS$_2$ in base oil would be beneficial for the design of novel MoS$_2$-based nano-additives for improving tribological performance in the industry and agriculture.

1. Introduction

Loss in materials and energies has been the major problem in modern industry, which could be mainly caused by friction and wear [1-5]. According to incomplete statistics, about 50% energies are dissipated in various forms during the friction and wear [6-8]. General speaking, liquid lubrication has been regarded as an ancient and effective way to reduce the frictional energy dissipation and promote mechanical performance [9-12]. Moreover, liquid-solid lubricating system consisted of base oil and solid additives can effective combine their advantages to control and reduce the machine parts against friction and wear, and further extend their usable life with the addition of lubricant additives [13-17]. In the past decades, nano-additives has got extensive attention as the most promising lubricant additives because of their excellent physicochemical properties, which contained with oil for enhancing the frictional performance compared to that of

---

* Corresponding author: xjing@ujs.edu.cn

traditional lubricant additives (e.g. commercial graphite and MoS_2) [9, 11, 12]. As a consequence, various inorganic nanoparticles including metal, metal oxides and sulfides, etc., have been extensive prepared as nano-additives due to their high abundance, low cost and excellent tribological property. However, the current challenges are how to seek and design novel inorganic nanoparticles or their composites for improving the anti-friction and wear resistance of lubricants [18-20].

To date, 2D layered materials represented by graphene and MoS_2 have been regarded as the most efficient lubricant additives for the present lubricating field due to lamellar structures and interlayer sliding owing to the weak van der Waals interactions within their molecular layers [21-25]. In the layered architecture of MoS_2, the sandwiched structure consisting of S–Mo–S layer could slide easily on the friction interface, leading to the decrease in friction coefficient and possess enhanced reducing-friction and anti-wear properties [26]. Many previous researches have also indicated nano-sized MoS_2 with different morphologies including nanorods, nanosheets, nanotubes, and nanospheres, etc., have excellent tribological performance using as lubricants compared with bulk MoS_2 [27-30]. Unfortunately, low dispersion and serious agglomeration of MoS_2 nanoparticles in base oil largely inherit their actual application in the field of lubricant and friction. For solving above problems, the modification and functionalization of MoS_2 nanomaterials is an urgent and critical task. Undoubtedly, nano-sized MoS_2 doped or coupled with other ceramic nanoparticles using as the nano-additives can enhance anti-friction and wear resistance of liquid lubricant. Very recently, MoS_2-incorporated nanocomposites consisted of MoS2 and other nanomaterials (e.g. graphene, CuO, TiO2 and ZnS, etc.) have been received extensive attention and synthesized through various methods, which also exhibited reinforcing and lubricating effects compared to that of pure MoS2.

As we know, titanium dioxide (TiO2) as a typical semiconductor has been extensive applied in energy and environmental fields due to its suitable electronic structure and optical performance [31-33]. Interestingly, TiO2 nanomaterials also possess superior corrosion resistance and frictional properties, and have been proven to be an ideal candidate for nano-lubricating additives owing to their low toxicity, good dispersion and robust stability in lubricant, and structural properties [34-36]. Furthermore, many recent reports have indicated MoS_2/TiO_2 system with excellent tribological properties is ascribe to the synergistic lubrication effect with the introduction of TiO2 nanoparticles [37-39]. For instance,

Motivated by previous reports mentioned above, we report the construction of $TiO_2@MoS_2$ heterojunction with in situ growth of TiO_2 nanoparticles coupled with MoS_2 nanospheres for improving reducing-friction and anti-wear properties via one-step hydrothermal approach using TiO_2 as the precursor, which were also systematically characterized. Subsequently, the tribological experiments were comparatively investigated by a ball-plate wear instrument using lubricating oil contained various nano-additive (e.g. TiO_2, MoS_2, and $TiO_2@MoS_2$). More importantly, the excellent anti-friction and wear-resistant of $TiO_2@MoS_2$ in base oil would be beneficial for the design of novel MoS_2-based nano-additives for improving tribological performance in the industry and agriculture.

2. Experimental section

2.1. Synthesis of TiO_2 nanoparticles

TiO_2 nanoparticles with high dispersion were fabricated through a hydrothermal approach of commercial titania (P25). For preparation, 1 g P25 powder dispersed into 30 mL NaOH solution (2 mlo/L) and continuous stirred for 1 h, then the above homogeneous solution was subsequently transferred into a 50 mL Teflon-lined stainless steel autoclave and maintained at 150 ℃ for 24 h. After that, the as-prepared samples were repeatedly washed with HCl solution (0.05 mol/L), DI water and ethanol and centrifuged. And the pH value of the above final solution was not less than 6.5. Finally, TiO_2 nanoparticles were obtained after drying (60 ℃, 8 h) and calcine process (450 ℃, 2 h).

2.2. Synthesis of $TiO_2@MoS_2$ heterojunction

$TiO_2@MoS_2$ heterojunction were fabricated by one-step hydrothermal approach using TiO_2 as the precursor. A certain amount of modified TiO_2 nanoparticles were added to 30 mL deionized water and continuous ultra-sonicated for 1 h. Then, $(NH_4)_2MoO_4 \cdot 4H_2O$ (0.8 g) and CH_4N_2S (3.6 g) were mixed with the above sonic solution, successively; and Polyvinylpyrrolidone (PVP) is used as a surfactant, which addition amount is 2.2 g. After strong agitation for 1h, the above suspension was subsequently transferred into a 50 mL Teflon-lined stainless steel autoclave and maintained at 180 ℃ for 24 h. Finally, $TiO2@MoS_2$ samples with various concentrations of TiO_2 were obtained after repeated washings with DI water and ethanol and drying at 60 ℃ in a vacuum oven for 8 h, which also was labeled as TM-1, TM-2, TM-3, TM-4, TM-5, and the addition amount of TiO_2 is 5%, 10%, 15%, 20%, 30%, respectively. Additionally, pure MoS_2 were prepared by the similar hydrothermal approach without the introduction of TiO_2 nanoparticles.

2.3. Characterization

XRD (Bruker-AXS), XPS (Thermo Scientific K-Alpha+ system), Raman Microscope (DXR-Thermo Scientific), SEM (JEOL JXA-840A) and TEM analysis (JEOL JEM-2100) are performed to investigate the phase compositions, chemical states and microstructure of the as-prepared products.

2.4. Tribological test

The friction reduction and anti-wear of pure base oil contained various nano-additives was investigated by a ball-on-disk tribometer (MS-T3001, China). In our experiments, liquid paraffin was selected as the lubricating oil. During experiments, the rotary velocity of the steel ball was kept 200 rpm, and the applied load was set to 2 N for 0.5 h at room temperature. Also, different tribological variables including the additive concentration (0.7-7 wt %), rotary velocity (100-500 rpm), and applied load (2-6 N) were investigated. More importantly, all friction experiments were investigated three times, respectively. Afterwards, the surface roughness and elemental composition of the worn surfaces were quantified by non-contact optical 3D profilers (SMP, NT1100, Veeco WYKO, USA), Atomic Force Microscopy (AFM, MFP-3D, USA), and SEM-EDS analysis (HITACHI S-3400N, Japan).

3. Results and discussion

The XRD patterns and Raman analysis of modified P25, MoS_2 nanospheres and $TiO_2@MoS2$ composites are illustrated in Fig. 1a. Clearly, all characteristic of modified P25 are well indexed to the standard card of Anatase (PDF#21-1272) and Rutile (PDF#21-1276) of TiO_2, respectively. And MoS_2 nanospheres show strong and broad peaks (e.g. (002), (100) and (110) plane) which is consistent with the standard card of hexagonal MoS_2 (JCPDS no. 37-1492).

Moreover, the sharp peak of (002) plane located at 16° was further indicated the stacking of MoS_2 layers. For $TiO_2@MoS_2$ composites, the typical peaks of TiO_2 and MoS_2 can be obtained which indicates the $TiO_2@MoS_2$ composite can be synthesized successfully by hydrothermal medication. Further to detect the presence of TiO_2 and MoS_2, the as-prepared $TiO_2@MoS_2$ composite ere also measured by Raman spectra, as shown Fig. 2. Obviously, two typical peaks located at 150 and 650 cm^{-1} are [40] assigned to rutile TiO_2, while the band at 400 and 520 cm^{-1} are consistent with anatase TiO_2. Furthermore, the Raman band located at 361.2 and 402.6 cm^{-1} corresponding to E^1_{2g} and A_{1g} modes of MoS_2. Additionally, the characteristic bands positions of TiO_2 and MoS_2 were coexisted in the Raman spectra of $TiO_2@MoS_2$, indicating the successful construction of $TiO_2@MoS_2$ [40-43].
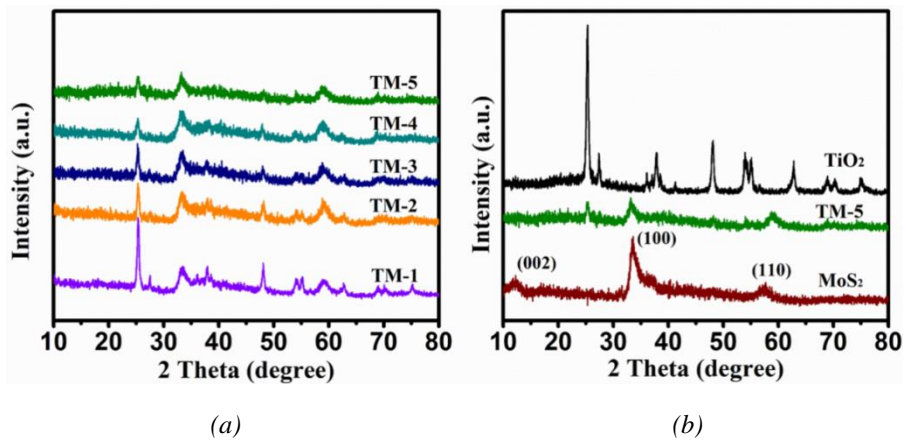

(a)   *(b)*

Fig. 1. XRD patterns of (a) TiO_2, $TiO_2@MoS_2$ composites and MoS_2 and (b) $TiO_2@MoS_2$ composites with different contents of TiO_2.
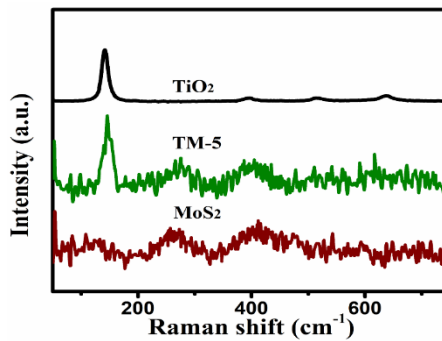

Fig. 2. Raman patterns of TiO_2, MoS_2 and $TiO_2@MoS_2$ composites.

SEM images of pure TiO_2, MoS_2 and TiO_2@MoS_2 composites are shown in Fig. 3. It can clearly be seen from SEM images that TiO_2 is asymmetric particle with an average size of 25 nm and present good dispersibility (Fig. 3a). And MoS_2 nanospheres with a size 100–150 nm is assembled by petal-like nanosheets, resulted in Fig. 3b. To TiO_2@MoS_2 composites (Fig. 3c and 3d), the similar ellipsoidal structures to MoS_2 are observed, and TiO_2 nanoparticles are distinctly dispersed in MoS_2 nanospheres.

(a)   *(b)*

(c)   *(d)*

Fig. 3. SEM images of (a) TiO₂, (b) MoS₂, (c) and (d) TiO₂@MoS₂ composites.

Further investigated by TEM, TiO_2 nanoparticles closely contact with flower-like MoS_2 nanospheres as shown Fig. 4a, which consistent with SEM results. Furthermore, HRTEM image of TiO_2@MoS_2 composites displayed the interplayer spacing of TiO_2 is 0.34 nm (Fig. 4b), which is in keeping with the (101) plane of anatase TiO_2. Compared with bulk MoS_2, the lattice fringes of (002) plane of MoS_2 layers is sufficiently expanded to 0.97 nm, which can be easier to interlayer slip.
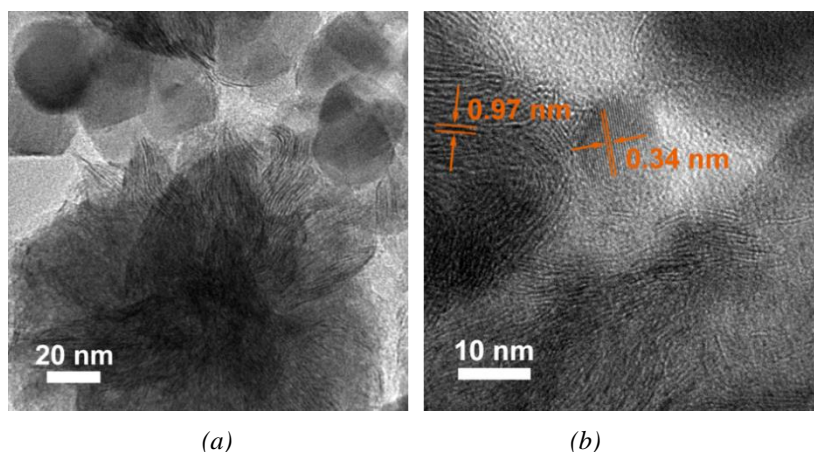
Fig. 4. (a) TEM image and (b) HRTEM image of $TiO_2@MoS_2$ composites.

The friction coefficients (COFs) of the as-prepared TiO_2, MoS_2, and $TiO_2@MoS_2$ contained with liquid paraffin were comparatively investigated by a ball-on-disk tribometer, and illustrated in Fig. 5. Obviously, the COFs of liquid paraffin containing various nano-additives exhibited lower friction coefficient compared to that of pure paraffin (Fig. 5a). With the introduction of $TiO_2@MoS_2$, the COFs of mixed oil gradually declined. Especially, 3%-$TiO_2@MoS_2$ samples exhibits further reduced COFs of 0.091, indicating the optimal addition; and its friction coefficient curve is stable and has slighter volatility (Fig. 5b). Furthermore, the tribological properties of $TiO_2@MoS_2$ for different applied loads and rotational speeds were also compiled. As the applied load increases, all COFs showed the trend which first decreased and then increased. By contrast, $TiO_2@MoS_2$ samples have lower friction coefficient compared with other mixed-oil samples. At the load of 5N, the COFs of $TiO_2@MoS_2$ samples were decreased to the minimum value (~0.08), as shown in Fig. 5c. Similarly, $TiO_2@MoS_2$ reveals excellent friction-reduction at high speed and low speed, resulted in Fig. 5d. Moreover, the experimental results of 300 rpm show the lowest COFs, as compared with other rotational speeds. Furthermore, the certain enhancement of friction coefficient of liquid paraffin contained $TiO_2@MoS_2$ is mainly attributable to the rise of interface temperature and damage of tribofilm.
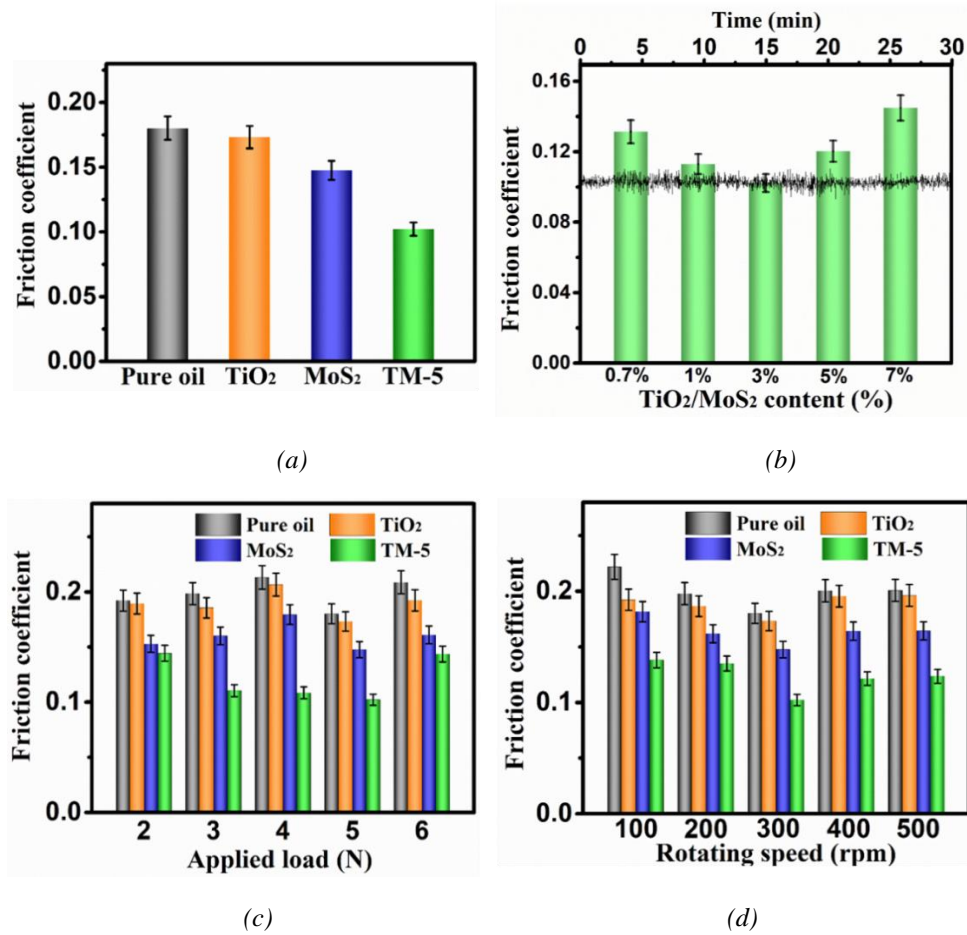
Fig. 5. (a) Friction coefficient of liquid paraffin contained with various oil additive; (b) Friction coefficient of liquid paraffin contained with different TiO₂@MoS₂ composites additive; Variations of mean friction coefficient of paraffin with different additive (c) increasing load (2-6 N), (d) under diverse speeds (100-500 rpm).

Fig. 6 show the wear scar morphology lubricated by liquid paraffin contained various nano-additives were investigated by SEM, respectively. Clearly, for pure liquid paraffin, some serious ploughing appear on the worn surface of steel disc (Fig. 6a). With the introduction of other nano-additives (e.g. TiO_2, MoS_2, $TiO_2@MoS_2$), the grinding crack on the surface of steel disc showed a declining trend, which wear scars were narrow and shallow, as shown Fig. 6 b-d. Moreover, SMP technology were further to detect 3D morphologies of friction interface and resulted in Fig. 7. As expected, SMP analysis also indicated the wear scar lubricated by liquid paraffin contained TiO2, MoS_2, and $TiO_2@MoS_2$ were relatively smooth, which exhibited no evident furrows cracks. As shown in Fig. 7a, the wear scar width and depth lubricated by pure paraffin are about 281 μm and 6.9 μm, while widths and depths of the wear tracks on the disk contained with TiO_2, MoS_2, and $TiO_2@MoS_2$ are reduced to 260 μm and 3.58 μm, 245 μm and 2.56 μm, and 1900 μm and 1.32 μm (Fig. 7b-d), respectively. Thus, the introduction of $TiO_2@MoS_2$ can efficiently limit further wear of contact surface and decrease contact area, resulting superior friction-reduction and anti-wear.
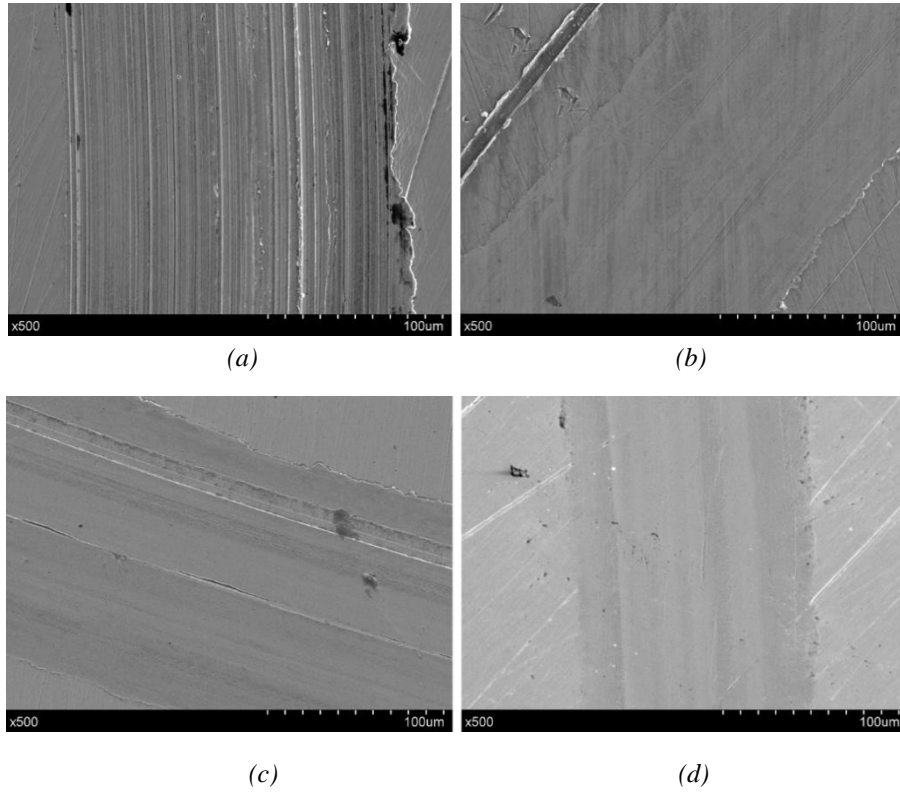
(a)   *(b)*

(c)   *(d)*

Fig. 6. SEM images of worn surfaces of (a) liquid paraffin, and liquid paraffin contained with (b) TiO2; (c) MoS$_2$ and (d) TiO$_2$@MoS$_2$ composites.

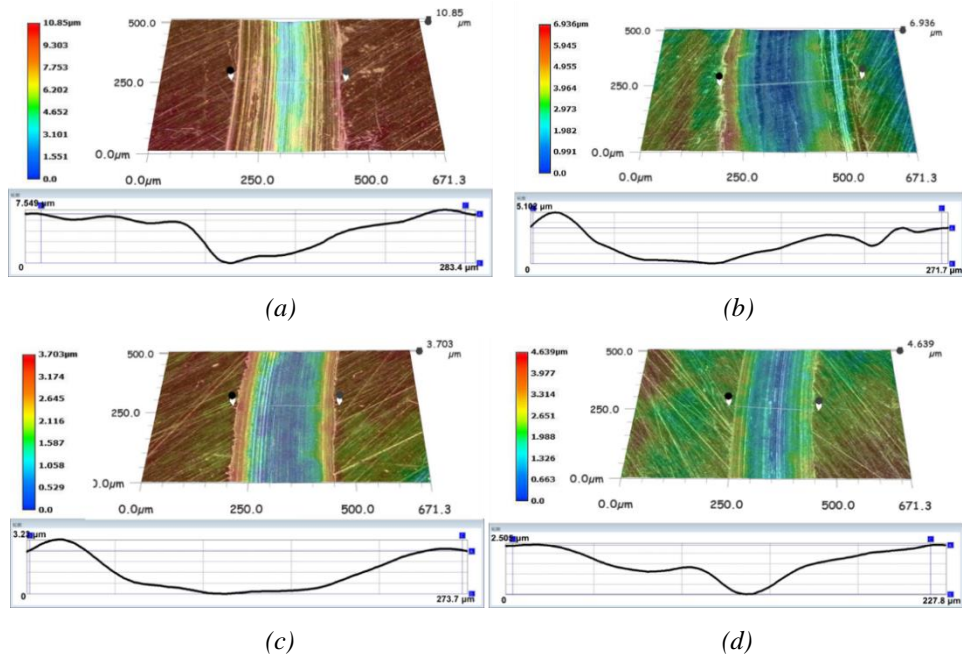*(a)*   *(b)*

(c)   *(d)*

Fig. 7. Noncontact three-dimensional images of worn surfaces of (a) liquid paraffin; and liquid paraffin contained with (b) TiO$_2$; (c) MoS$_2$ and (d) TiO$_2$@MoS$_2$ composites.

Further to study antifriction and transfer mechanisms of $TiO_2@MoS_2$-oil system, AFM image and EDS analysis were performed to quantify the surface roughness and elemental composition of the worn surfaces, resulting in Fig. 8.
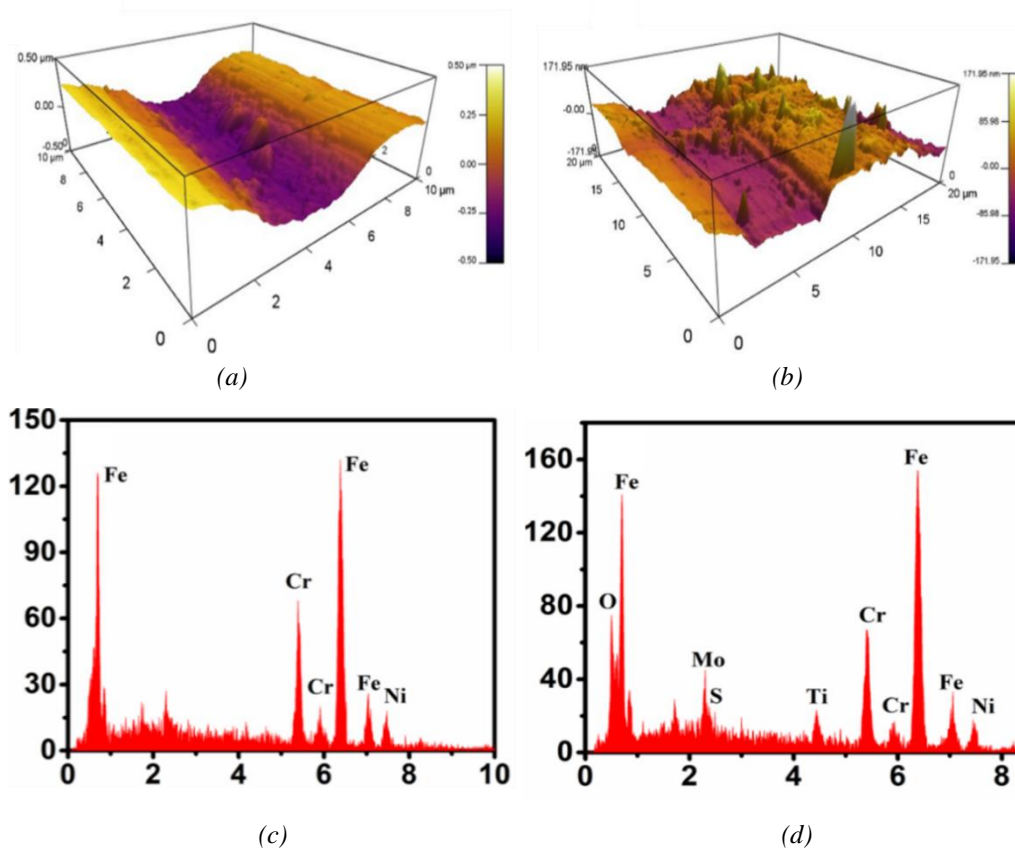

(a)   *(b)*

(c)   *(d)*

Fig. 8. AFM images and EDS analysis of worn surfaces of liquid paraffin (a, c)
and (b, d) $TiO_2@MoS_2$ composites

After lubricated by pure paraffin, the maximum roughness of worn surfaces is approximately 0.5 μm, and many deep furrows and wear debris are observed (Fig. 8a). By the use of liquid paraffin containing with $TiO_2@MoS_2$ nanoparticles (Fig. 8b), its maximum roughness was decreased to 172 nm, which has a slight irregular scuffing consisting of smoother and shallower peaks and valleys. Furthermore, EDS results indicate Mo, S, Ti and O elements were obtained inside the tribofilm of worn surfaces lubricated by paraffin-$TiO_2@MoS_2$ system (Fig. 8d). On the contrary, the worn surfaces of pure paraffin is mainly consisted of Fe, Cr and Ni elements, and no other elements (e.g. Mo, S, Ti and O) are observed (Fig. 8c). Moreover, the above results also indicate $TiO_2@MoS_2$ nanoparticles can be transferred to the contact surface and formed the tribo-film during the friction process, which can efficiently promote anti-friction and wear-resistant of lubricating oil.

4. Conclusions

In summary, $TiO_2@MoS_2$ nano-additives consisted of TiO_2 nanoparticles and MoS_2 nanospheres were successfully fabricated by one-step hydrothermal approach using TiO_2 as the

precursor, which was applied directly as a novel lubrication additive for tribological studies of liquid paraffin. The characterization results indicate that TiO_2 nanoparticles with an average size of 25 nm were homogeneously decorating flower-like MoS_2 nanospheres with diameter of about 100-150 nm.

Furthermore, the tribological experiments were investigated by a ball-plate wear instrument, which reveals $TiO_2@MoS_2$ as an additive in base oil exhibited superior antifriction and wear resistant among various nano-additives. At the optimal conditions, 5%-$TiO_2@MoS_2$-paraffin samples show the lower friction coefficient (~0.08) compared with pure paraffin, and paraffin contained TiO_2 and/or MoS_2. Therefore, TiO_2 nanoparticles modified MoS_2 will be beneficial for the design of novel MoS_2-based nano-additives for improving tribological performance in the industry and agriculture.

Acknowledgements

References

[1] L. Chen,Y.-Z. Sun, L. Li, Y.-P. Ren, X.-D. Ren, Appl. Surf. Sci. **518**, 145981 (2020).

[2] H. Li, S.-B. Lu, P.-Y. Xu, L. Jiao, J.-J. Yang, D.-G. Wu, Mater. Res. Express **7**, 056510 (2020)

[3] X.-F. Lu, J.-B. Li, X.-H. Chen, J.-W. Qiu, Y. Wang, B. Liu, Y. Liu, M. Rashad, F.-S. Pan, Intermetallics **120**, 106758 (2020).

[4] Q.-N. Song, Y. Tong, N. Xu, S.-Y. Sun, H.-L. Li, Y.-F. Bao, Y.-F. Jiang, Z.-B. Wang, Y.-X. Qiao, Wear **450**, 203258 (2020).

[5] Y.-H. Zhang, Y.-H. Fu, X.-J. Hua, L. Quan, J.-J. Qu, Wear **448**, 203216 (2020).

[6] J.-Y. Gu, R.-F. Li, S.-G. Chen, Y.-H. Zhang, S.-J. Chen, H. Gu, Materials **13**, 1611 (2020).

[7] K. Xiang, L.-Y. Chen, L. Chai, N. Guo, H. Wang, Appl. Surf. Sci. **517**, 146214 (2020).

[8] Y.-F. Yan, Z.-J. Meng, H. Liu, J.-Z. Wang, B.-B. Chen, F.-Y. Yan, Tribol. Int. **144**, 106117 (2020).

[9] X.-H. Jia, J. Huang, Y. Li, J. Yang, H.-J. Song, Appl. Surf. Sci. **494**, 430 (2019).

[10] J. Li, H. Yin, C. Zhai, A. Wang, L. Shen, J. Appl. Polym. Sci. **136**, 47168 (2019).

[11] F.-X. Zhang, G.-G. Tang, J. Xu, C.-S. Li, Micro Nano Lett. **14**, 1355 (2019).

[12] F.-X. Zhang, X.-Y. Zhang, F.-L. Zhang, G.-G. Tang, C.-S. Li, J. Xu, Mater. Res. Express **6**, 1250f9 (2019).

[13] L.-Z. Li, J.-L. Jiang, R.-H. Wei, J.-P. Li, Y. Tian, J.-N. Ding, Acta Physica Sinica **65**, 018103 (2016).

[14] Z.-P. Wang, L. Qian, Z.-X. Jiang, X. Xue, K. Reddy, AIP Adv. **10**, 045013 (2020)

[15] Z.-L. Xie, N.-W. Shen, W.-D. Zhu, H.-L. Liu, J. Shi, Y.-K. Wang, W.-C. Tian, Ann. Nucl. Energy **136**, 107059 (2020).

[16] F. Yan, Z.-Y. Wang, Y.-C. Du, S.-J. Su, Y. Zheng, Q.-F. Li, Ind. Lubr. Tribol. **69**, 1066 (2017).

[17] J. Yang, Y.-F. Xia, H.-J. Song, B.-B. Chen, Z.-Z. Zhang, Tribol. Int. **105**, 118 (2017).

[18] H. Fu, G. Yan, M. Li, H. Wang, Y. Chen, C. Yan, C.-T. Lin, N. Jiang, J. Yu, RSC Adv. **9**, 42481 (2019).

[19] X. Li, B.-B. Chen, Y.-H. Jia, X.-F. Li, J. Yang, C.-S. Li, F.-Y. Yan, Surf. Coat. Tech. **344**, 154 (2018).

[20] S. Zhang, J. Yang, B.-B. Chen, S. Guo, J.-F. Li, C.-S. Li, Surf. Coat. Tech. **326**, 87(2017).

[21] B.-B. Chen, Y.-H. Jia, M.-J. Zhang, H.-Y. Liang, X. Li, J. Yang, F.-Y. Yan, C.-S. Li, Compos. Part A: Appl. S **122**, 85 (2019).

[22] H.-Y. Liang, M.-J. Xu, Y.-F. Bu, B.-B. Chen, Y.-H. Zhang, Y.-H. Fu, X.-J. Xu, J.-Y. Zhang, Appl. Surf. Sci. **485**, 64 (2019).

[23] B.-B. Chen, X. Li, Y.-H. Jia, X.-F. Li, J. Yang, F.-Y. Yan, C.-S. Li, Compos. Part A: Appl. S **109**, 232 (2018).

[24] B.-B. Chen, X. Li, Y.-H. Jia, X.-F. Li, M.-S. Zhang, J.-Z. Dong, J. Compos. Mater. **52**, 2631 (2018).

[25] Y.-M. Zeng, F. He, L.-N. Si, Y.-J. Wang, Q. Wang, Mater. Res. Express **6**, 1150b4 (2019).

[26] Y.-M. Zeng, F. He, Q. Wang, X.-H. Yan, G.-X. Xie, Appl. Surf. Sci. **455**, 527 (2018).

[27] P. Basumatary, D. Konwar, Y. S. Yoon, Appl. Catal. B-Environ **267**, 118724 (2020).

[28] J. Dai, J. Balamurugan, N. H. Kim, J. H. Lee, J. Alloys Compd. **825**, 154085 (2020).

[29] H. Fu, X.-D. Zhang, J.-Z. Fu, G.-Z. Shen, Y.-L. Ding, Z.-J. Chen, H. Du, J. Alloys Compd. **829**, 154557 (2020).

[30] J.-H. Liu, P.-P. Chen, F.-Q. Xia, Z. Liu, H.-B. Liu, J.-L. Yi, C.-L. Zhou, Sens. Actuators B Chem. **315**, 128098 (2020).

[31] J. Wang, G.-H. Wang, J. Jiang, Z. Wan, Y.-R. Su, H. Tang, J. Colloid Interface Sci. **564**, 322 (2020).

[32] R. Wang, J. Shen, K.-H. Sun, H. Tang, Q.-Q. Liu, Appl. Surf. Sci. **493**, 1142 (2019).

[33] R. Wang, J. Shen, W.-J. Zhang, Q.-Q. Liu, M.-Y. Zhang, Zulfiqar, H. Tang, Ceram. Int. **46**, 23 (2020).

[34] Y.-H. Feng, J.-H. Fang, J. Wu, K.-C. Gu, P. Liu, Tribol. Int. **146**, 106233 (2020).

[35] P.-F. Huang, R.-T.Zhu, C.-Y. Li, X. Wang, X. Wang, X.-X. Zhang, Mater. Design **188**, 108468 (2020).

[36] B. Li, Y.-M. Gao, X.-H. Hou, C. Li, H.-J. Guo, Y.-C. Kang, Y.-F. Li, Q.-L. Zheng, S.-Y. Zhao, Tribol. Int. **144**, 106108 (2020).

[37] K.-H. Hu, Y. Xu, E.-Z. Hu, J.-H. Guo, X.-G. Hu, Tribol. Int. **104**, 131 (2016).

[38] Z.-Y. Xu, Y. Xu, K.-H. Hu, Y.-F. Xu, X.-G. Hu, Tribol. Int. **81**, 139 (2015).

[39] W. Zheng, W.-P. Jia, L. Deng, B.-X. Wang, Y. Tian, A.-T. Zhang, L. Mao, J.-Q. Liu, W.-L. Zhang, J. Mater. Chem. C **6**, 1836 (2018).

[40] C.-F. Zhong, W. Weng, X.-X. Liang, D. Gu, W. Xiao, Appl. Surf. Sci. **507**, 145072 (2020).

[41] Y.-C. Du, X.-M. Zhang, L.-Q. Wei, B. Yu, Y.-H. Wang, Y.-L. Wang, S.-F. Ye, Mater. Chem. Phys. **241**, 122448 (2020).

[42] Y.-K. Li, P. Zhang, D.-Y. Wan, C. Xue, J.-T. Zhao, G.-S. Shao, Appl. Surf. Sci. **504**, 144361 (2020).

[43] W.-Z. Xiao, L. Xu, Q.-Y. Rong, X.-Y. Dai, C.-P. Cheng, L.-L. Wang, Appl. Surf. Sci. **504**, 144425 (2020).